International Journal of Crashworthiness
Vol. 14, No. 2, April 2009, 125–138

Taylor & Francis
Taylor & Francis Group

A comparative study of design optimisation methodologies for side-impact crashworthiness, using injury-based versus energy-based criterion

M.F. Horstemeyer,[a,b*] X.C. Ren,[a] H. Fang,[c] E. Acar,[d] and P.T. Wang[a]

[a]*Center for Advanced Vehicular Systems, Mississippi State University, Mississippi State, Mississippi, USA;* [b]*Mechanical Engineering Dept, Mississippi State University, Mississippi State, Mississippi, USA;* [c]*Mechanical Engineering and Engineering Science, University of North Carolina, Charlotte, North Carolina, USA;* [d]*Mechanical Engineering Department, Sogutozu Ankara, Turkey*

(*Received 17 September 2008; final version received 30 September 2008*)

The tension between occupant safety during a crash and lightweight designs continues to be an important driver of modern vehicle designs. While occupant safety may be defined and evaluated in various ways, maximising energy absorption of structural components during impact has been adopted for vehicle designs by many manufacturers. An alternative method to evaluate safety but often not directly used in the design of structural components is the use of a dummy model in the finite element (FE) simulation to estimate the forces and accelerations that would be experienced by a human in a crash environment. This paper investigates the similarities/differences between designing vehicular structural components experiencing side impacts based upon two different criteria: (1) the energy absorption of collapsed components in the absence of a dummy and (2) an injury metric–based approach with the responses of the dummy as the bases. Multi-objective optimisation methods are used with finite element analysis (FEA) in the lightweight design for side-impact crashworthiness, considering the two different criterion. The results show that the optimum designs based on the two criteria are significantly different and that the injury-based approach should be incorporated into vehicular lightweight design process when considering crashworthiness.

Keywords: energy absorption; injury evaluation; dummy; multi-objective optimisation; side impact; metamodelling; finite element analysis; crash

1. Introduction

Improving occupant safety continues to be an important field in vehicle designs. Statistics from the National Highway Traffic Safety Administrations (NHTSA) shows that six million vehicle crashes occurred in the United States in the year 2006, which injured more than two and half million people and claimed more than 40,000 lives. Among the injured or killed, more than half were passengers in cars. Furthermore, side impacts appear to be more damaging to humans than other crash scenarios. At the same time, lightweight passenger cars, which meet fuel economy needs, have become more attractive to customers. With lighter weight vehicles, safety has become one of the major concerns; thus, automotive designers are striving to maintain the crashworthiness of vehicle structures while reducing the mass of vehicle components.

During the past several years, vehicle designs based on energy absorption [4, 10, 15] were introduced into passenger vehicles to meet both demands on crashworthiness and fuel economy. Energy absorption for reducing injury of occupants generally favours a less stiff structure; however, excessive reduction of stiffness also reduces crashworthiness due to the increased risk of occupant injury by excessive intrusion into sensitive areas such as the passenger cabin. On the other hand, a design based on energy absorption typically focuses on the amount of energy that can be dissipated among structural components but tends to omit occupant responses that may cause injuries during the impact.

To evaluate occupant safety and reduce the potential for injury during crashes, mechanisms of occupant injury and factors affecting injury potential were fairly recently investigated [1, 16, 18]. The development of a dummy finite element (FE) model [8, 11, 12, 14] makes it possible to evaluate injuries in different kinds of crash scenarios. Both crash simulations and statistical data show that the chest and pelvis are regions of the human body most likely to be injured in a side impact. Furthermore, the US New Car Assessment Program (NCAP), as mandated by the Federal Motor Vehicle Safety Standard (FMVSS) for passenger protection, requires the injury potentials to the chest and pelvis be evaluated by accelerations to the dummy rib, lower spine and pelvic region [13, 17].

The goal of this study is to systematically evaluate two different criteria for vehicular crashworthiness designs for a side impact: energy absorption by structural components and injury to the dummy. With the objective of minimising weight and a constraint on the lateral intrusion distance, the designs based on both criteria were evaluated under

*Corresponding author. Email: mfhorst@me.msstate.edu

ISSN: 1358-8265

DOI: 10.1080/13588260802539489
http://www.informaworld.com

the same side-impact scenarios. The optimisation in this study used the thicknesses of side-door components as design variables and thus is a size optimisation problem. To reduce the computational costs of optimisation, involving expensive crash simulations, the radial basis function (RBF) [2, 5, 6, 7] approximations of objective and constraint functions were adopted. The structure of the paper is as follows: the side-impact simulation models are first introduced in Section 2. Details of RBF metamodelling are then presented in Section 3, followed by the optimisation formulations given in Section 4. Finally, the comparison and discussion on simulation results based on the two criteria are given in Section 5.

2. Side-impact simulations with and without dummy

2.1. Two side-impact finite element analyis (FEA) meshes

Two kinds of side-impact meshes were used in this study, and they are illustrated in Figure 1: a dummy-interactive mesh and a mesh without a dummy. Both side-impact simulations were achieved by a moving deformable barrier (MDB), with all wheels rotated 27° from the longitudinal axis, impacting a stationary test vehicle with a 54 km/h (33.5 miles/h) closing speed. For a typical passenger car, the left edge of the MDB is 940 mm (37 in.) ahead of the midpoint of the impacted vehicle wheel base. The MDB has a total mass of 1367 kg (3015 lbs). The aluminium honeycomb of the barrier face is specified by design. The bottom edge of the MDB is 280 mm (11 in.) from the ground. The protruding portion of the barrier simulating a bumper is 330 mm (13 in.) from the ground.

The effects of the steering wheel and the seat were considered in both types of FE simulations. In the dummy-interactive FEA simulations, the MDB impacted near the side of the occupant. The meshes without the dummy and with the dummy comprised 232,062 and 230,274 shell elements, respectively. In these simulations we will examine as metrics for optimisation the energy absorption and dummy response for the simulation with the dummy and compare them to the energy absorption of the simulation without the dummy. Not much difference is anticipated with the energy absorption in the two types of simulations, but the comparison will be made if the dummy interaction with the door affects the energy absorption of the structural components.

2.2. Simulation results

Figures 2 and 3 illustrate the response of the dummy-interactive simulation at 100 ms. Significant deformation is observed in the side door on the left and B-pillars, which are the main structural components that absorb the energy from the MDB during side impact. The significant displacement of the dummy signifies the considerable impact to the dummy, although the large deformation of the side doors and B-pillars are designed to mitigate the energy to the interior (Figure 3). Note that these simulations do not have side airbags. A top view of the side-impact simulation results, showing the deformation history, is shown at times 0 ms, 20 ms, 40 ms, 60 ms, 80 ms and 100 ms in Figure 4. Although these simulations appear to be similar, minor nuances occur

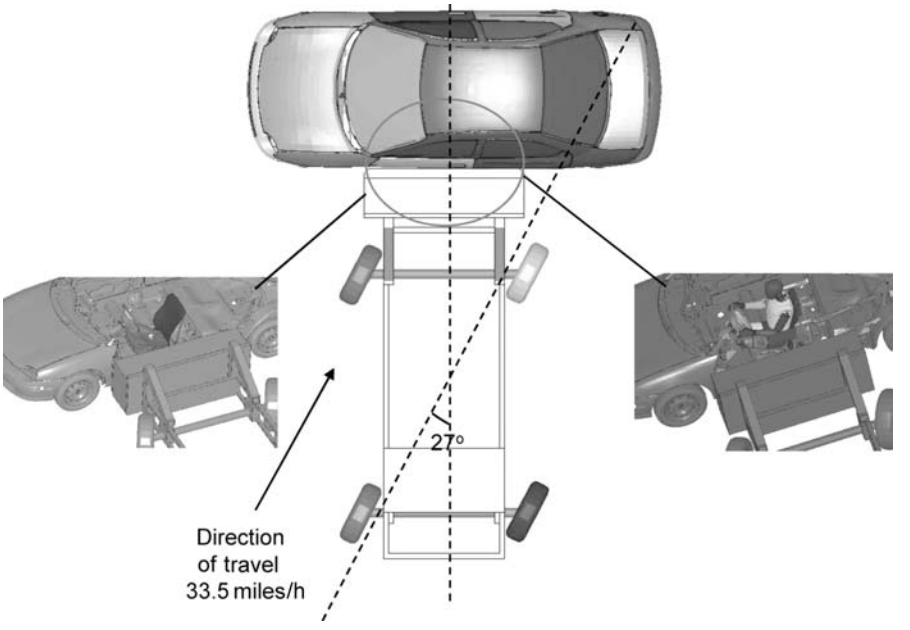

Figure 1. Two kinds of side-impact FE simulations: one without the dummy and one with the dummy.

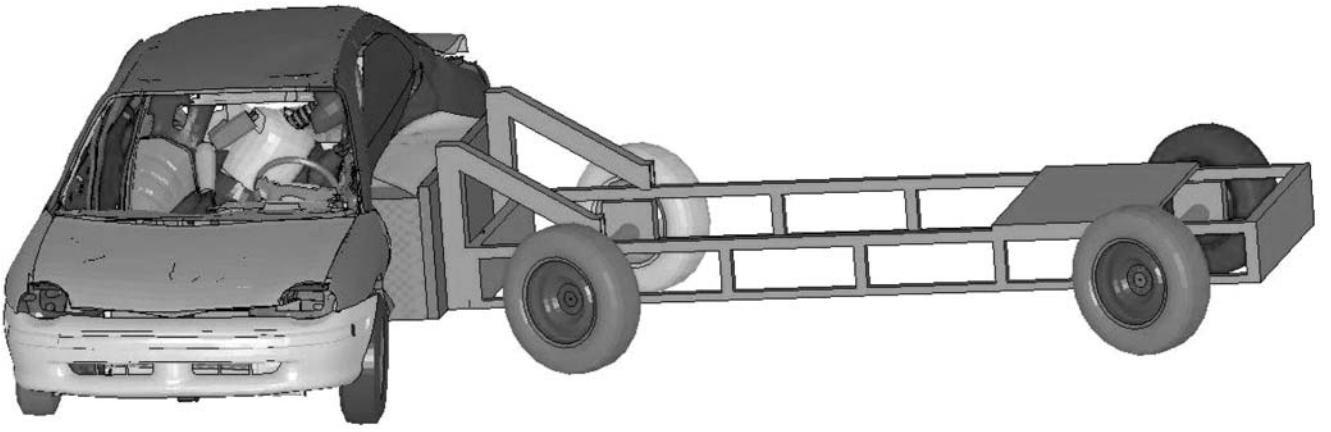

Figure 2. FE side-impact results of the dummy-interactive model.

that illustrate a different response as will be dicussed later. Similar to Figure 4, Figure 5 shows a frontal view of the displacement and deformation history of the dummy and side-door parts during side impact at times 0 ms, 20 ms, 40 ms, 60 ms, 80 ms and 100 ms.

3. RBF metamodelling

Even with an increased capability of parallel computing clusters and the efficiency of solvers, the evaluation of these two (FE) impact simulations can still take many CPU hours on parallel computing environments. One of

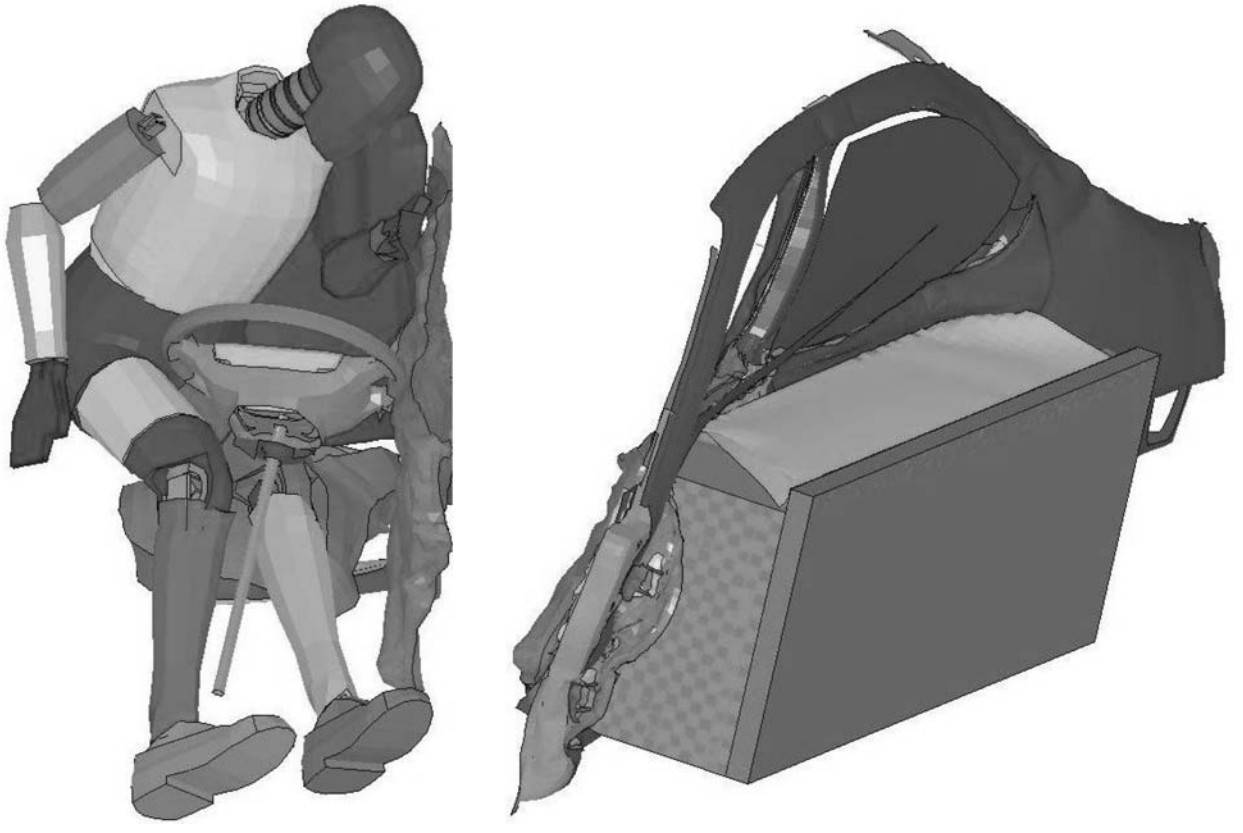

Figure 3. Dummy movement and deformation of the side door under a side-impact FE simulation.

the more popular approaches for the economical usage of such expensive simulations is to combine optimisation algorithms, inexpensive global approximation metamodels and the high-fidelity computational simulations. Among the extensively used metamodelling technologies, the response surface methodology (RSM), which adopts polynomials,

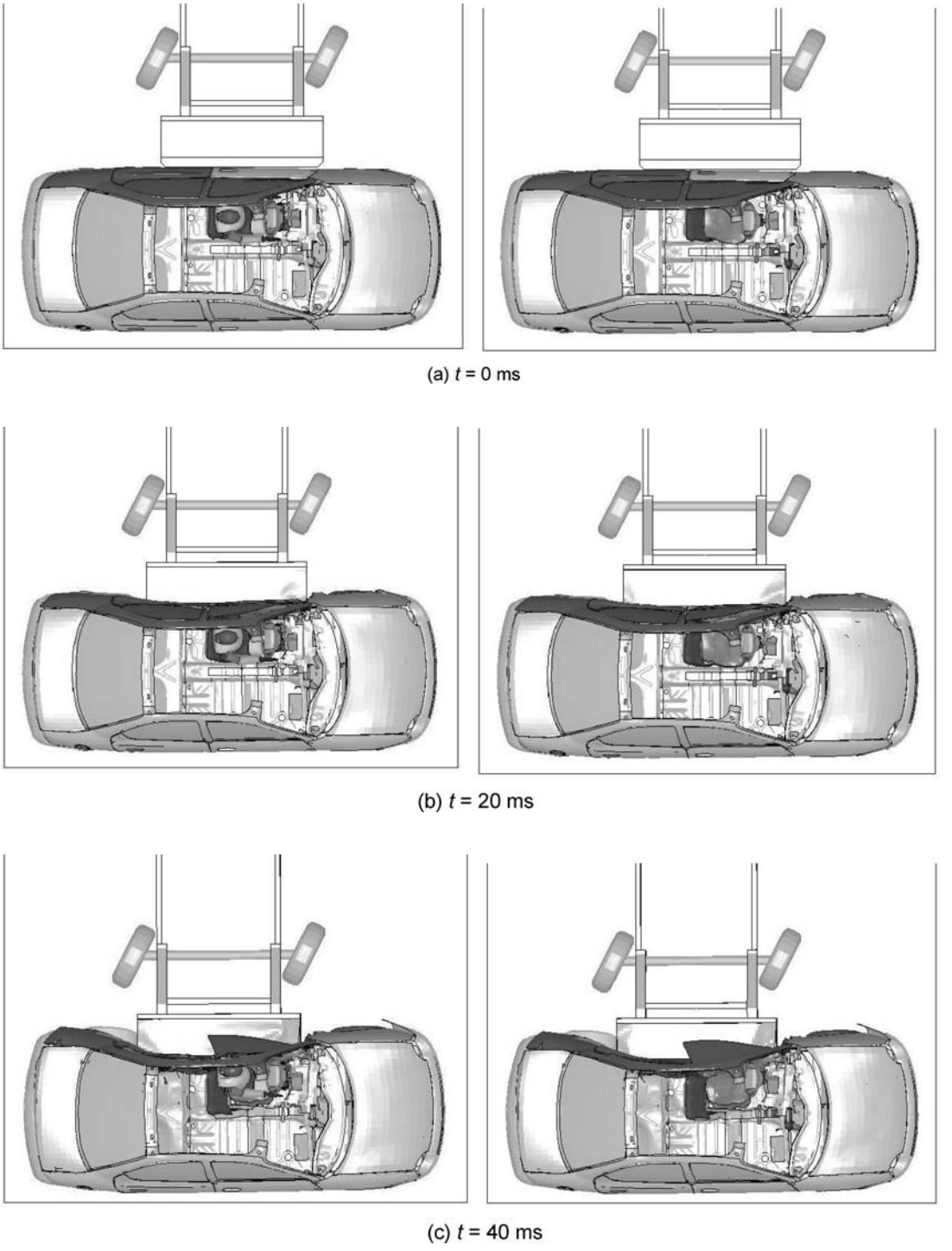

Figure 4. Top view of side-impact results of the dummy-interactive model and the model without the dummy at (a) 0 s, (b) 20 ms, (c) 40 ms, (d) 60 ms, (e) 80 ms and (f) 100 ms.

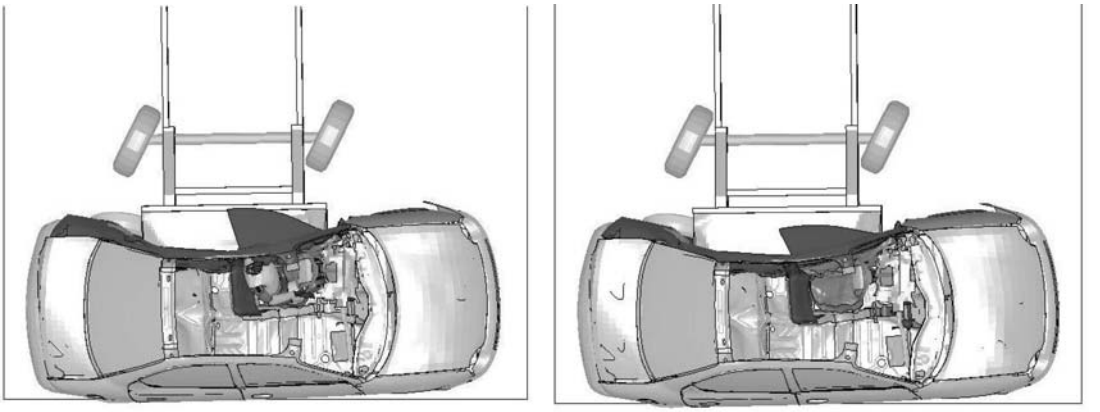

(d) t = 60 ms

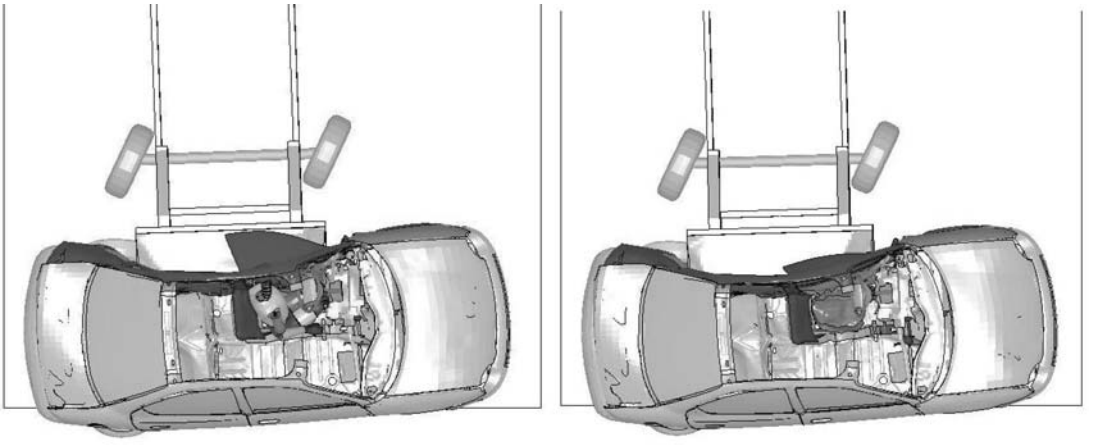

(e) t = 80 ms

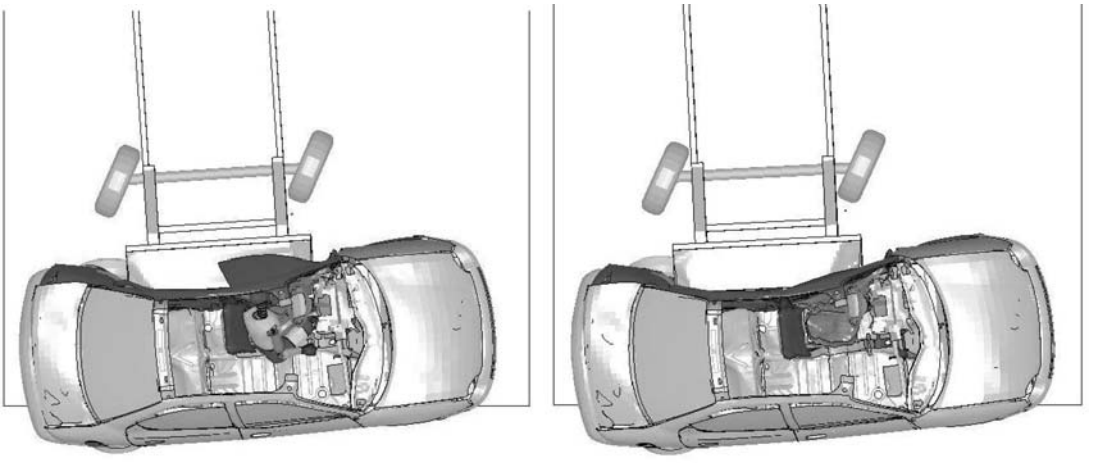

(f) t = 100 ms

Figure 4. *Continued*.

has been used in various non-linear complex boundary value problems [2, 3, 5, 7, 9]. Jin et al. [6] showed that an RBF had a better performance based on different measures of error than RSM, kriging method (KM) and multivariate adaptive regression splines (MARS) for both small-scale and large-scale problems. Fang et al. [2, 3, 5, 7, 9], compared a variety of existing basis functions in both non-augmented and augmented RBF metamodels with various

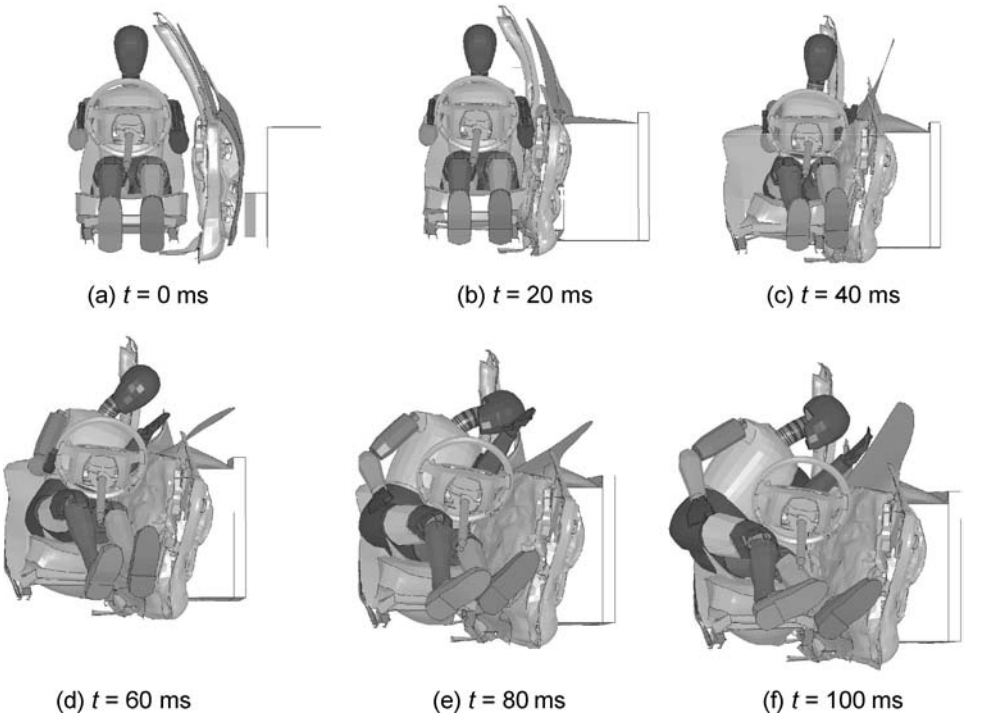

Figure 5. FE simulation results of the sequence of dummy movement during the side impact at (a) 0 s, (b) 20 ms, (c) 40 ms, (d) 60 ms, (e) 80 ms and (f) 100 ms.

types of responses and a limited numbers of samples. They showed that the augmented RBF models with compactly supported base functions, created by Wu [19], are the best for both low- and high-order non-linear responses. In this section, a brief review of RBF metamodelling is given.

The approximation of real function $f(\mathbf{x})$ using an augmented RBF can be expressed as follows:

$$\hat{f}(\mathbf{x}) = \sum_{i=1}^{n} \lambda_i \phi(\|\mathbf{x} - \mathbf{x}_i\|) + \sum_{j=1}^{m} c_j p_j(\mathbf{x}), \tag{1}$$

where ϕ is the radial basis function; $\|\|$ denotes the Euclidean norm; $\mathbf{x}_i$ is the coordination vector of the ith sampling point; p_j are polynomial basis functions; and λ_i and c_j are the weighted coefficients for the radial basis functions and polynomial basis functions, respectively. To solve these undetermined parameters (λ_i and c_j) from an interpolation perspective, $m + n$ sampling points are required. To reduce the number of sampling points, the following orthogonality conditions are introduced without loss of generality:

$$\sum_{i=1}^{n} \lambda_i p_j(\mathbf{x}_i) = 0 \qquad \text{for } j = 1, 2, ..., m. \tag{2}$$

So now, only n sampling points are needed to determine the parameters of the metamodel. The n sampling points and corresponding real function values form n equations. Combined with the m orthogonal conditions, the following equation set can be obtained:

$$\begin{bmatrix} \mathbf{\Phi} & \mathbf{P} \\ \mathbf{P_T} & \mathbf{0} \end{bmatrix} \begin{bmatrix} \boldsymbol{\lambda} \\ \mathbf{c} \end{bmatrix} = \begin{bmatrix} \mathbf{f} \\ \mathbf{0} \end{bmatrix}. \tag{3}$$

The matrices $\mathbf{\Phi}$ and $\mathbf{P}$ are determined by the sampling point function value of the radial basis function and the polynomial basis function, respectively.

4. Energy absorption design and injury design

In this section, two optimisation metrics are used for the energy absorption design and injury-based design of a 1996 Dodge Neon car under a side impact. The intrusion distances are considered as constraints in both optimisation models.

4.1. Energy absorption redesign methodology

$$\min[f_w(\mathbf{x}), f_{ea1}(\mathbf{x}), f_{ea2}(\mathbf{x}), f_{ea3}(\mathbf{x}), f_{ea4}(\mathbf{x}), f_{ea5}(\mathbf{x})],$$
$$s.t. \quad g_{id}(\mathbf{x}) - d \le 0,$$
$$\underline{\mathbf{x}} \le \mathbf{x} \le \overline{\mathbf{x}},$$

where $f_w(\mathbf{x})$ is the total weight of the design components; $f_{eai}(\mathbf{x})$ is the total internal energy of design components at times 20 ms, 40 ms, 60 ms, 80 ms and 100 ms; $g_{id}(\mathbf{x})$ is the maximum value of the lateral intrusion distance; $\underline{\mathbf{x}}$ and $\overline{\mathbf{x}}$ are the lower and upper bounds of design variables; and d is the constraint for the lateral intrusion.

4.2. Injury-based redesign methodology

Research on injury patterns in side impacts [1, 16] shows that the head, thorax and pelvis are the main injury locations and are exposed to a high fatal severity during side impact. In NCAP for side-impact protection, the pelvic injury is evaluated by the peak lateral acceleration of the pelvis, and the injury potential to the chest is evaluated by thoracic trauma index (TTI):

$$TTI = \frac{(a_r + a_{LS})}{2},$$

where a_r is the greater of the peak accelerations of either the upper or the lower rib and a_{LS} is the lower spine peak acceleration.

Referring to the above literature, we give

$$\begin{aligned} &\min\left[f_w(\mathbf{x}), f_{a1}(\mathbf{x}), f_{a2}(\mathbf{x}), f_{a3}(\mathbf{x})\right], \\ &s.t. \quad g_{id}(\mathbf{x}) - d \le 0, \\ &\quad \underline{\mathbf{x}} \le \mathbf{x} \le \overline{\mathbf{x}}, \end{aligned}$$

where $f_{a1}(\mathbf{x})$ is the maximum lateral acceleration observed at the head; $f_{a2}(\mathbf{x})$ is the maximum lateral acceleration observed at the spine; and $f_{a3}(\mathbf{x})$ is the maximum lateral acceleration observed at the pelvis over the course of the simulations (100 ms).

Table 1. The structural components and associated design part with corresponding variation.

DV	Part no.	Variation	Name
x_1	236,237	20%	Outer-door front thickness
x_2	272,273	20%	Outer-door back thickness
x_3	224,225	20%	Side-impact bar front
x_4	254,255	20%	Side-impact bar back-low
x_5	256,257	20%	Side-impact bar back-up
x_6	328,329	20%	Middle B-pillar
x_7	326,327	20%	Inner B-pillar
x_8	234,235	20%	Inner door front
x_9	266,267	20%	Inner door back

4.3. Design variables and corresponding components

The design variables in both design methods are shown in Table 1. As shown in the 'variation' column, $\underline{\mathbf{x}} = \mathbf{x} - 0.2\mathbf{x}$ and $\overline{\mathbf{x}} = \mathbf{x} + 0.2\mathbf{x}$. The components to be redesigned are shown in Figure 6.

In Sections 4.1 and 4.2, d is the constraint for the lateral intrusion $g_{id}(\mathbf{x}) - d \le 0$ and could be the maximum intrusion d_0 obtained from the FEA simulation without a dummy (like the original design) or the maximum intrusion d_1 obtained from the dummy-interactive FEA model. In the following section, various comparisons are given, and $d = d_i\,(i = 0, 1)$ is adopted to distinguish the two different intrusion constraints. All implicit functions for

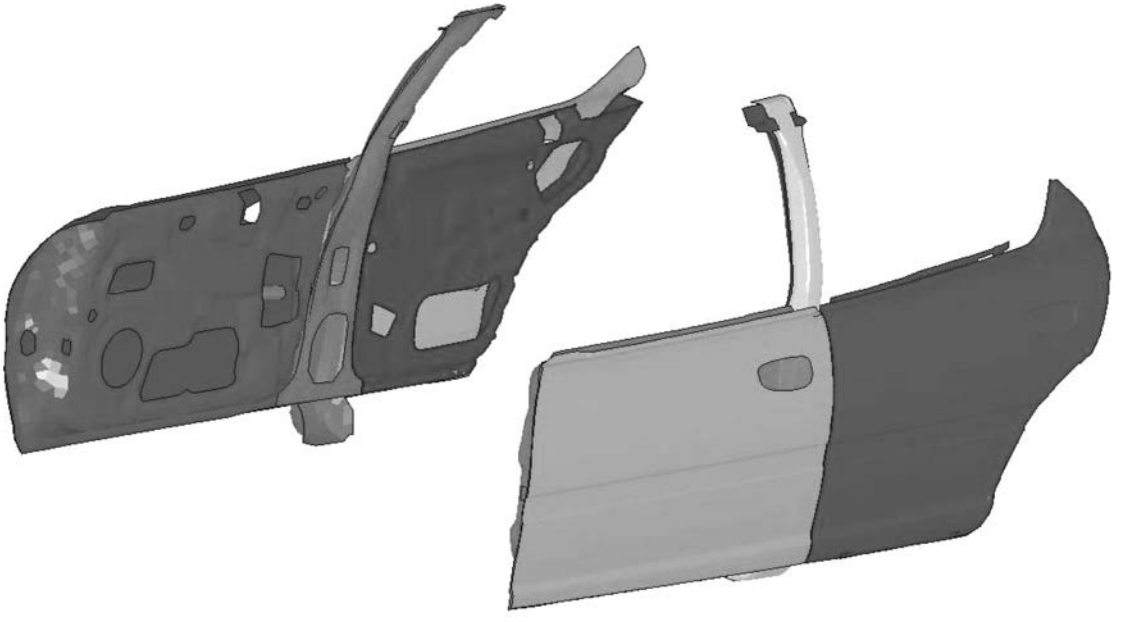

Figure 6. The structural components of the Dodge Neon considered for redesign.

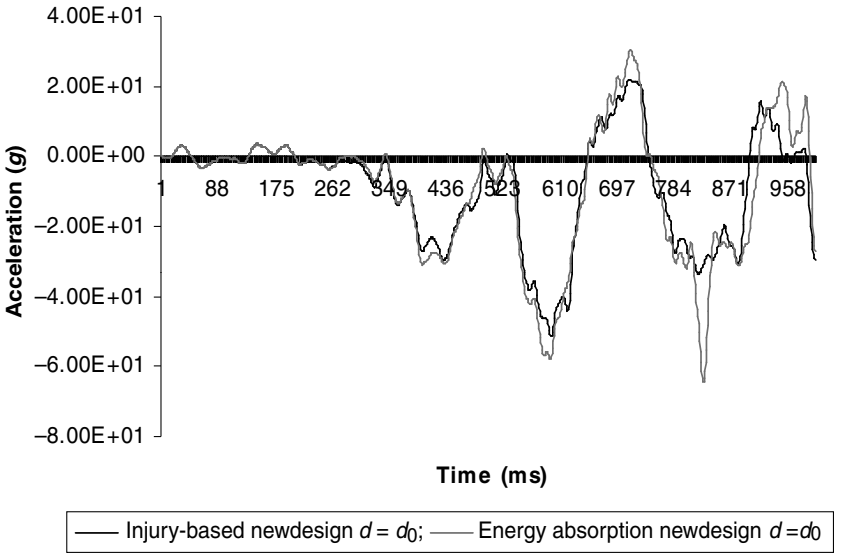

Figure 7. Maximum lateral accelerations of the *head* during side impact after redesign.

both optimisation methods are approximated by RBF metamodelling, using 50 sampling points generated by the Taguchi method.

5. Comparison of the optimised designs

The two new designs based on the dummy injury metric and the energy absorption of the structural components metric were then simulated in LS-Dyna to evaluate the effect of the optimised designs. Along with the first-order metrics mentioned, we also used the intrusion distance as a constraint for the side impact.

5.1. Maximum lateral acceleration of critical redesigned structural components

Figures 7–9 compare the two new designs based upon the injury metric and the energy absorption metric in which the dummy was inserted into both new designs. Note that by examining the maximum lateral accelerations to the head, spine and pelvis, respectively, in each of the figures, some differences were observed. Although the new energy absorption design increased the internal energy absorption capacity, which is shown in Figure 10, the maximum lateral accelerations were much larger than accelerations from the

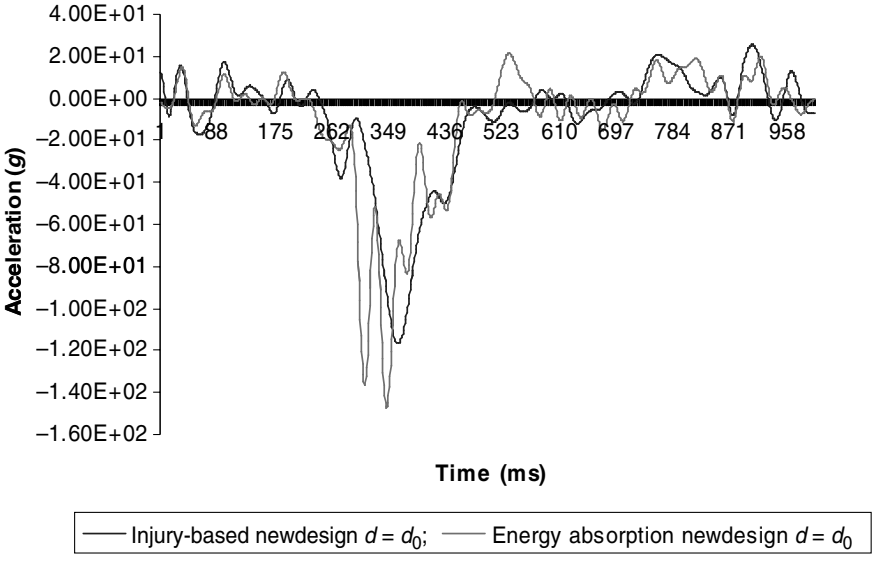

Figure 8. Maximum lateral accelerations of the *spine* during side impact after redesign.

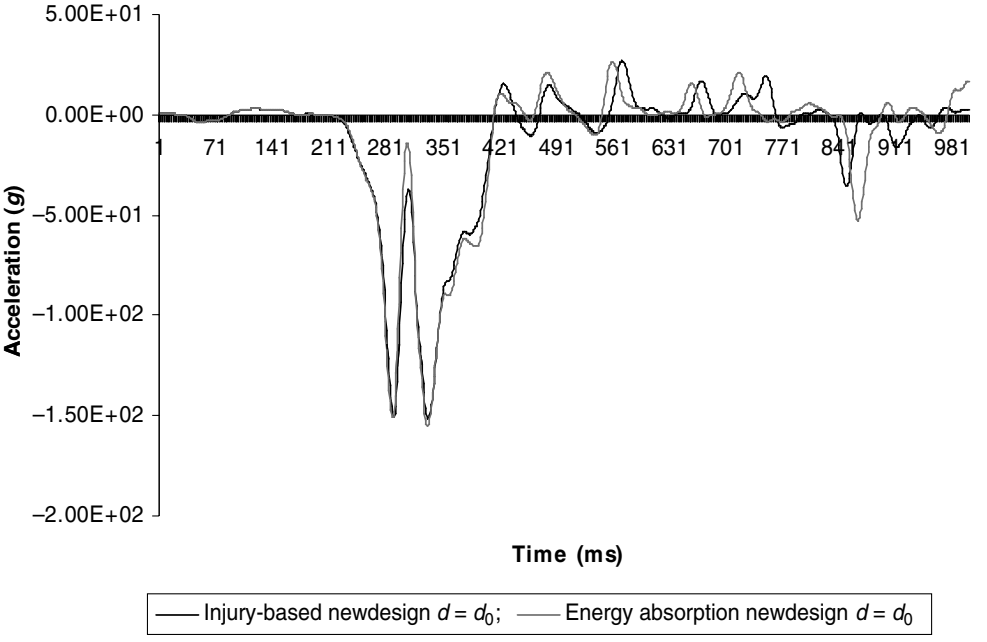

Figure 9. Maximum lateral acceleration of the *pelvis* during side impact after redesign.

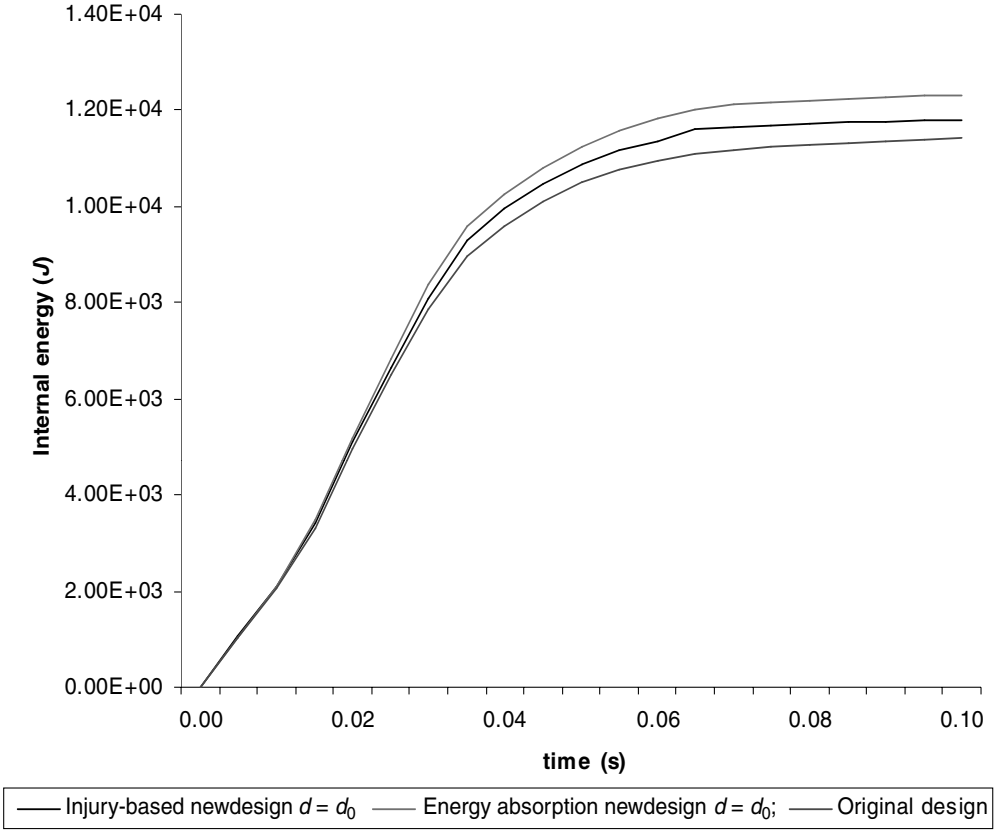

Figure 10. Internal energy history after redesign.

Table 2. The structural components and associated design part with corresponding variation.

Design variables	Energy absorption design $d = d_0$ ($\times\ t_0 \times 20\%$)	Injury-based design $d = d_0$ ($\times\ t_0 \times 20\%$)	Original design thickness t_0 (mm)
x_1 variation	1.0000	9.9909e-1	0.8460
x_2 variation	1.0000	−9.9805e-01	0.8270
x_3 variation	−1.0000	−9.9805e-01	2.6900
x_4 variation	−1.0000	1.0000	2.6270
x_5 variation	−1.0000	1.0000	2.2000
x_6 variation	1.0000	4.7024e-01	0.7060
x_7 variation	−1.0000	9.9805e-01	1.3280
x_8 variation	−1.0000	1.0000	0.6780
x_9 variation	−1.0000	2.4555e-01	0.6820
Total mass of all design parts (ton)	0.0426 (−2% difference)	0.0453 (+4% difference)	0.0436

new injury-based design. In Figure 7, depicting the head response, one can see that at approximately 825 ms, the new injury metric design experienced an acceleration of 33 gs but the new energy absorption design experienced twice as many gs (66). Clear differences were found in the spine and the pelvis as well, which are shown in Figures 8 and 9, respectively. Clearly, this result indicates that the energy-absorption criterion for a design methodology will not generate the 'safest' door.

The mass of energy absorption, injury-based design and original design are shown in Table 2 for comparision. One can see that the injury-based design had two major components that effected change upon the system mass in the same way: the B-pillar middle structure and the inner-door back structure.

5.2. Design trends of the two design methods and the two FEA models

In Section 4, the new minimum weight designs were adopted to compare both the new injury-based design with the new energy absorption design and the influence of the dummy in the two different FE simulations. Since the optimisation problems discussed in this research are multi-objective in nature, an exact comparison for the redesign results may be misleading. As such this section is written to disclose the different trends of the optimisation

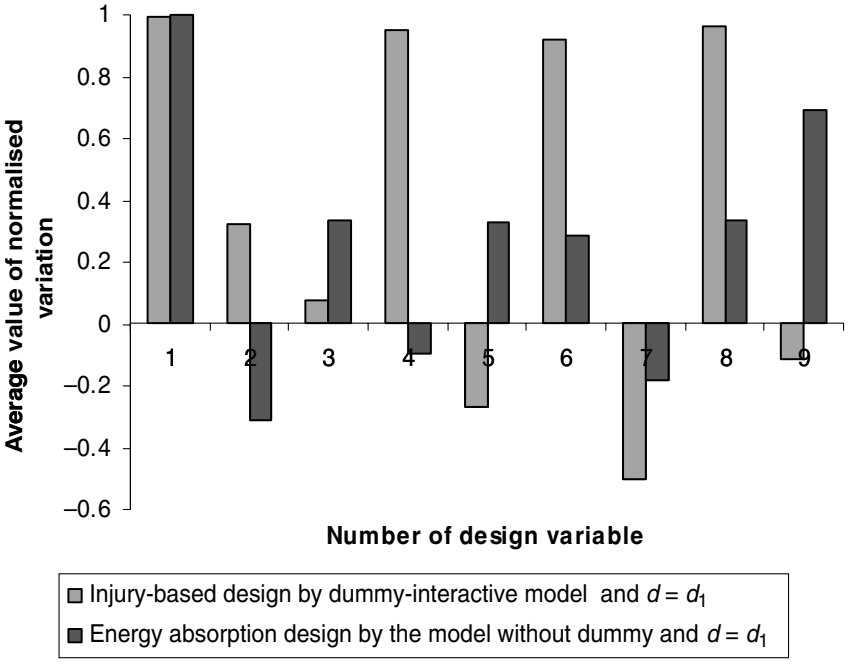

Figure 11. Comparison of the average of effective solution sets of the new designs.

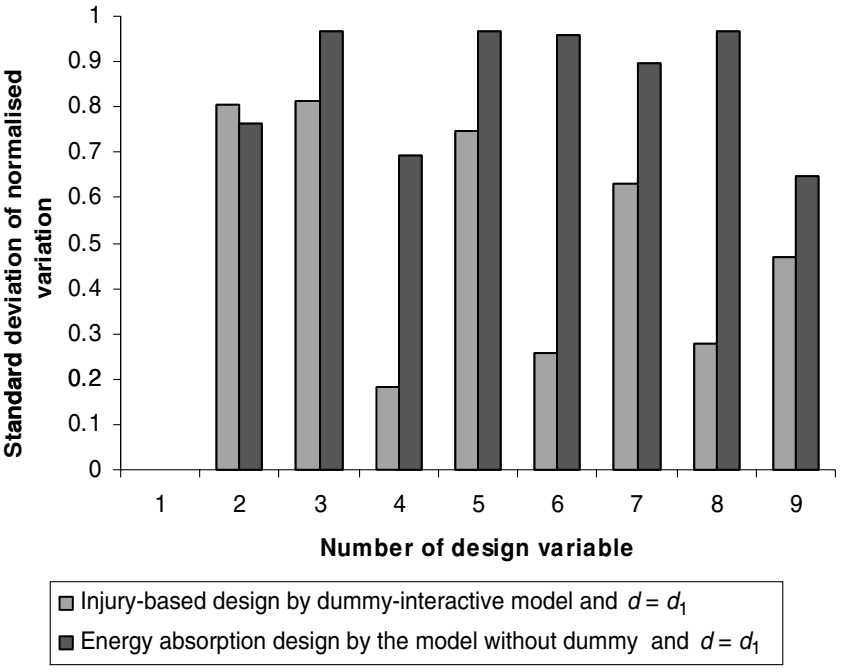

Figure 12. Comparison of the standard deviations of effective solution sets of the new designs.

methodologies by comparing the mean values and standard deviations of effective solution sets.

The new injury-based design of the nine structural components with the dummy-interactive FE simulation and the new energy absorption–based design with the FE simulation without a dummy are compared in Figures 11 and 12. Both the new injury-based design and the new energy absorption–based design demand that the thicknesses of outer parts of front doors, whose mean value is 1 and standard deviation 0, take the upper bound of a feasible interval. For the new injury-based design, there is a strong trend to maximise the thicknesses of the lower side-impact bar of

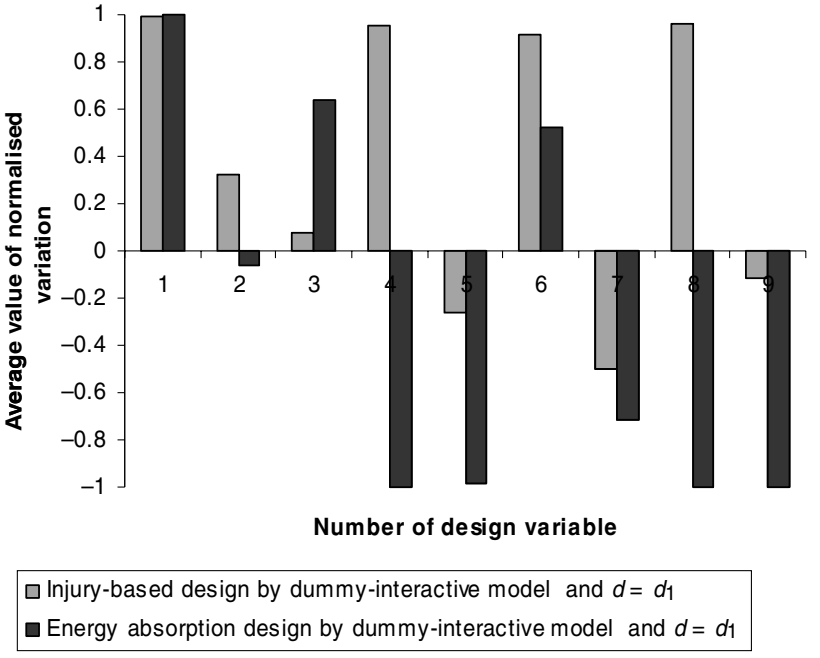

Figure 13. Comparison of the average of effective solution sets of the new designs.

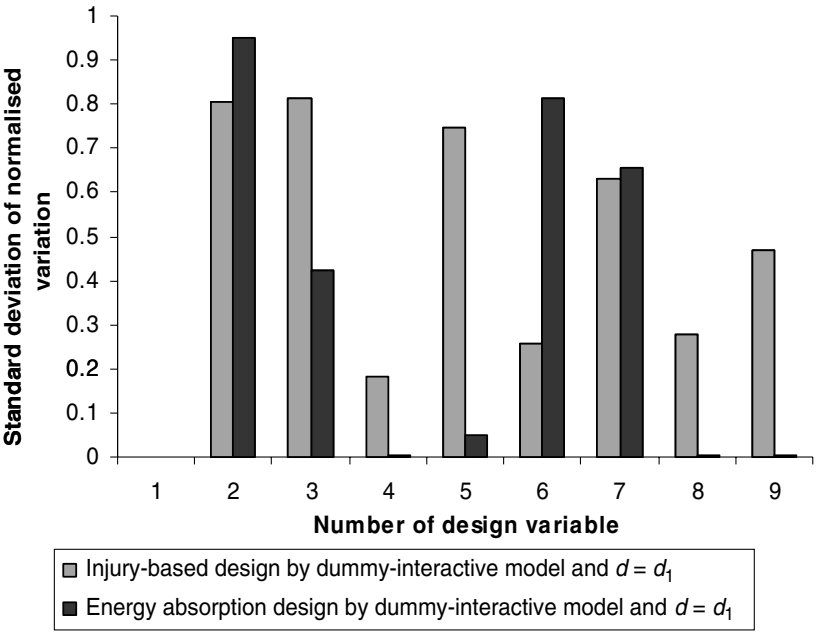

Figure 14. Comparison of the standard deviations of effective solution sets of the new designs.

the back doors, the middle B-pillar and the inner parts of the front door, which yield a large mean value and a small standard deviation.

Another trend was that the new energy absorption design when using the dummy-interactive FEA simulation minimised the thicknesses of the lower and upper side-impact bars of the back doors and the inner parts of the back and front doors, which are shown in Figures 13 and 14. Figures 15 and 16 compare the averages and standard deviations of the design variables, using the new

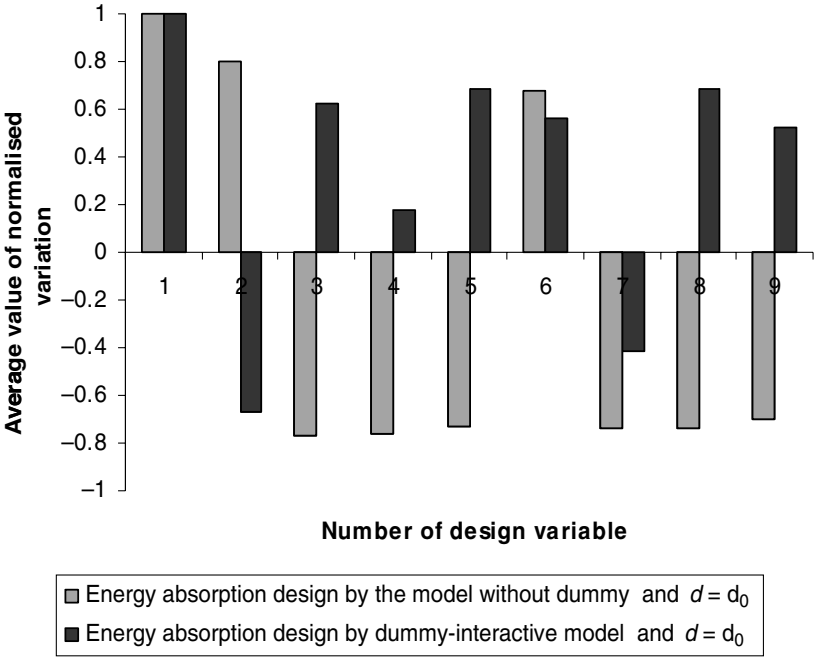

Figure 15. Comparison of the average of effective solution sets of the new designs.

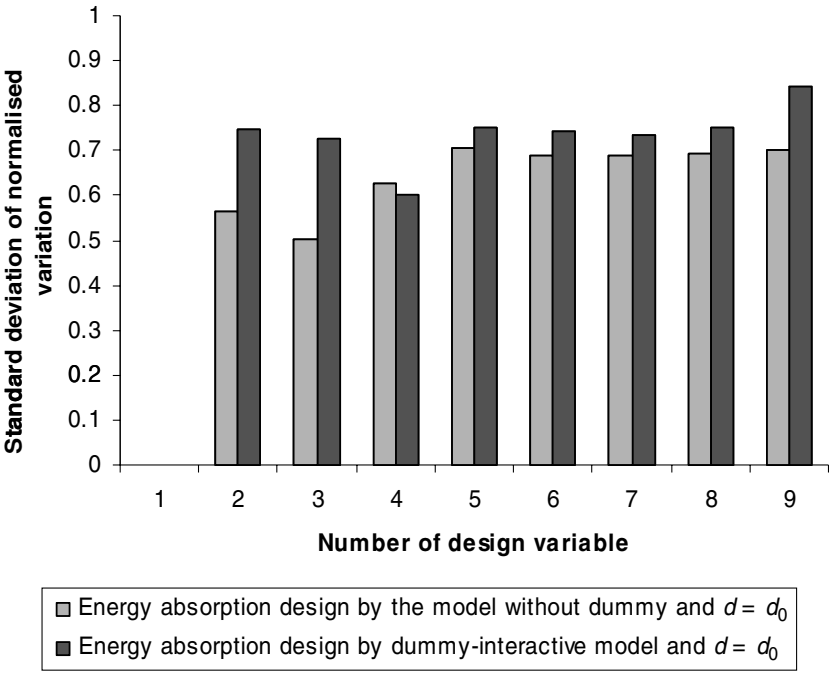

Figure 16. Comparison of the standard deviations of effective solution sets of the new designs.

energy absorption design metric for the two kinds of FEA simulations (with and without the dummy) with an intrusion distance upper bound d_0. The only small deviation parts are the outer parts of the front doors, which show that the same design trend on this part is the maximisation of the thickness.

6. Conclusions

In this paper, the thicknesses of nine 1996 Dodge Neon structural components were optimised by solving two different multi-objective optimisation problems: one that employed an injury-based metric and one that employed an energy absorption metric. The injury-based metric was based upon accelerations to a dummy, and the energy-absorption metric was focused upon structural components. The current methodologies of design and redesign typically focus on energy absorption, where the dummy is not present. Dummy-interactive FEA simulations and FEA simulations without a dummy under side-impact loading conditions were employed for the optimisation analyses. The main findings of this study are as follows:

(1) The maximum mass reduction solutions for the new energy absorption design induced a higher lateral acceleration to the head and the spine of a dummy than the maximum mass reduction solutions for the new injury-based design. As such, the new injury-based design metric is a much safer design than the new energy absorption design metric.

(2) The difference between the dummy-interactive FEA simulations and the FEA simulations without a dummy resulted in different thicknesses of the middle and inner B-pillars under the same multi-optimisation method (energy absorption metric). The dummy-interactive FEA simulation was more realistic than the model without a dummy, since the mass of the dummy and contacts between the car and the dummy were included.

(3) The outer part of the front door was the only part for which the thickness was the maximum value for the new designs. As such, the redesign for this component was necessary and independent of the two types of FEA simulations and the two multi-objective metrics presented in this paper.

(4) Different multi-objective optimisation methods always minimised the thicknesses of certain, but different, structural components to reduce the weight; the injury-based design increased the stiffness of the lower side-impact bars of the back doors, the middle B-pillar and the inner structure of the front door. Quite distinct from the injury-based design, the new energy-absorption design maintained the stiffness of most of the structural components.

Acknowledgements

This study was supported by the Center for Advanced Vehicular Systems (CAVS) at Mississippi State University (MSU) and the Department of Energy (DOE) under contract no. DEFC2606NT42755.

References

[1] S. Acierno, R. Kaufmanc, F.P. Rivara, D.C. Grossman, and C. Mock, *Vehicle mismatch: Injury patterns and severity*, Accid. Anal. Prev. 36 (2004), pp. 761–772.

[2] M.D. Buhmann, *Radial Basis Functions: Theory and Implementations*, Cambridge University Press, New York, 2003.

[3] H. Fang, M. Rais-Rohani, Z. Liu, and M.F. Horstemeyer, *A comparative study of metamodeling methods for multiobjective crashworthiness optimization*, Comput. Struct. 83 (25–26) (2005), pp. 2121–2136.

[4] H. Fang, K. Solanki, and M.F. Horstemeyer, *Numerical simulations of multiple vehicle crashes and multidisciplinary crashworthiness optimization*, Int. J. Crashworthiness 10 (2) (2005), pp. 161–171.

[5] H. Fang and M.F. Horstemeyer, *A generic optimizer interface for programming-free optimization systems*, Adv. Engg. Software 37 (6) (2006), pp. 360–369.

[6] H. Fang and M.F. Horstemeyer, *Global response approximation with radial basis functions*, Engg. Optimiz. 38 (4) (2006), pp. 407–424.

[7] H. Fang and M.F. Horstemeyer, *HIPPO: An object oriented framework for general purpose design optimization*, J. Aero. Comput. Inform. Commun. 2 (2005), p. 490.

[8] P.A. Forbes, D.S. Cronin, and Y.C. Deng, *Multi-scale human body model to predict side impact thoracic trauma*, Int. J. Crashworthiness 11 (3) (2006), pp. 203–216.

[9] M.F. Horstemeyer, H. Fang, and K. Solanki, *Energy-based crashworthiness optimization for multiple vehicle impacts*, Transportation 2004: Transportation and Environment 11–16 (2004), p. 2005.

[10] P. Hosseini-Tehrani and M. Nikahd, *Proceedings of the Institution of Mechanical Engineers: Part D; Effects of ribs on S-frame crashworthiness*, J. Automob. Engg. 220 (d12) (2006), pp. 1679–1689.

[11] M. Iwamoto, K. Miki, and K.H. Yang, *Development of a finite element model of the human shoulder to investigate the mechanical responses and injuries in side impact*, JSME Int. J.: Series C; Mechanical Systems Machine Elements and Manufacturing 44 (4) (2001), pp. 1072–1081.

[12] C.D. Kan, D. Marzougui, G.T. Bahouth, and N.E. Bedewi, *Crashworthiness evaluation using integrated vehicle and occupant finite element models*, Int. J. Crashworthiness 6 (3) (2001), pp. 387–397.

[13] R. Kent and J. Crandall, *International harmonization of side impact standards: vehicle design and thoracic injury criteria trends*, Int. J. Vehicle Des. 32 (1–2) (2003), pp. 158–172.

[14] S. Majumder, A. Roychowdhury, and S. Pal, *Dynamic response of the pelvis under side impact load: A three-dimensional finite element approach*, Int. J. Crashworthiness 9 (1) (2004), pp. 89–103.

[15] W.G. Qi, X.L. Jin, and X.Y. Zhang, *Improvement of energy-absorbing structures of a commercial vehicle for crashworthiness using finite element method*, Int. J. Adv. Manuf. Technol. 30 (11–12) (2006), pp. 1001–1009.

[16] S. Kumaresan, A. Sances, Jr., F. Carlin, R. Frieder, K. Friedman, and D. Renfroe, *Biomechanics of side impact injuries: Evaluation of seat belt restraint system, occupant kinematics and injury potential*, in Proceedings of the 28th IEEE EMBS Annual International Conference, New York City, USA, Institute of Electrical and Electronics Engineers Inc., 2006.

[17] A.F. Tencer, R. Kaufman, C. Mack, and C. Mock, *Factors affecting pelvic and thoracic forces in near-side impact crashes: A study of US-NCAP, NASS, and CIREN data*, Accid. Anal. Prev. 37 (2) (2005), pp. 287–293.

[18] L. Thollon, C. Cavallero, M. Py, and P.C. Brunet, *The thoracic member under side impact: An experimental approach*, Int. J. Crashworthiness 6 (3) (2001), pp. 307–319.

[19] Z. Wu, *Compactly supported positive definite radial functions*, Adv. Comp. Math. 4 (1995), pp. 283–292.